

NJC

Accepted Manuscript



This is an *Accepted Manuscript*, which has been through the Royal Society of Chemistry peer review process and has been accepted for publication.

Accepted Manuscripts are published online shortly after acceptance, before technical editing, formatting and proof reading. Using this free service, authors can make their results available to the community, in citable form, before we publish the edited article. We will replace this *Accepted Manuscript* with the edited and formatted *Advance Article* as soon as it is available.

You can find more information about *Accepted Manuscripts* in the [Information for Authors](#).

Please note that technical editing may introduce minor changes to the text and/or graphics, which may alter content. The journal's standard [Terms & Conditions](#) and the [Ethical guidelines](#) still apply. In no event shall the Royal Society of Chemistry be held responsible for any errors or omissions in this *Accepted Manuscript* or any consequences arising from the use of any information it contains.



NJC

ARTICLE

Pulse reverse electrodeposited NiCo₂S₄ nanostructures as efficient counter electrodes for dye-sensitized solar cells

Krishnan Shanmugam Anuratha, Subramanian Mohan* and Subhendu K. Panda*

Received 00th January 20xx,
Accepted 00th January 20xx

DOI: 10.1039/x0xx00000x

www.rsc.org/

Dendritic nanostructures of NiCo₂S₄ were deposited on a transparent conducting glass substrate by facile one step electrodeposition method and are used as counter electrodes (CEs) for the dye-sensitized solar cells (DSSCs). The NiCo₂S₄ thin films were deposited by both potentiostatic (PS) and pulse reverse (PR) electrodeposition techniques and characterized by using X-ray diffraction (XRD), scanning electron microscopy (SEM), electrochemical impedance spectroscopy (EIS) and cyclic voltammetry (CV). Both PS and PR techniques produced dendrite like NiCo₂S₄ nanostructures. CV and EIS measurements revealed the excellent electrocatalytic activities in the I⁻/I₃⁻ redox reaction for DSSCs. Sequential CV scanning further showed the high electrochemical stability of the NiCo₂S₄ dendritic nanostructures. The CEs prepared by PR and PS technique displayed power conversion efficiency of 7.03 % and 6.01 % respectively, which are better than the control device with thermal decomposed Pt. Due to the large surface area of the NiCo₂S₄ dendrite structures and high electrocatalytic activity towards the reduction of I₃⁻ to I⁻, the electrodes demonstrated high solar cell conversion efficiency. This simple and low cost electrodeposition technique shows promise for large scale production of environment friendly and highly efficient NiCo₂S₄ CEs for DSSC applications.

1. Introduction

Dye-Sensitized Solar Cells (DSSCs) have been viewed as one of the most anticipating alternatives for the traditional silicon solar cells since the first report by Grätzel et.al in 1991.¹ The conventional DSSC holds a sandwich structure with a photoanode which is anchored by dye molecules, an iodide/triiodide (I⁻/I₃⁻) redox couple electrolyte and a counter electrode (CE)². To enhance the efficiency of DSSCs, a lot of modifications on photoanode, dye, electrolyte and CE have been reported.³⁻⁷ One of the most essential components for a long-term operation of the DSSC is the counter electrode and it should have a low charge transfer resistance, high exchange current densities, chemical and electrochemical stability in the electrolyte system. So far, platinum has been the preferred material for the CE due to its excellent electrocatalytic activity and stability towards (I⁻/I₃⁻) redox couple. Mostly, platinum CE is fabricated by thermal decomposition of chloroplatinic acid solution or sputtering of Pt on fluorine doped tin oxide (FTO) glass substrates, but the cost of Pt and heat treatments are the limiting factor for the large scale application and commercialization of DSSCs. Hence it is highly essential to replace the Pt with other alternative material.⁸

Recent literatures demonstrated the various options for

substituting Pt such as carbonaceous materials^{9, 10}, conducting polymers,¹¹ transition metal sulphides,¹² carbides¹³ and nitrides.¹⁴ The binary transition metal sulphides such as NiS,¹⁵ CoS,¹⁶ MoS₂¹⁷ and WS₂¹⁸ have been proposed as the alternative materials to replace the Pt CE for not only being electrocatalytic activity but also having a high corrosion resistance property. Multi-metal sulfide based CEs such as CuInS₂ and Cu₂ZnSnS₄ (CZTS) have been exhibited excellent performance than Pt in DSSCs and quantum dot sensitized solar cells (QDSSCs).^{19, 20} In recent years, more and more attention has been given to ternary transition metal sulphides in various applications.²¹⁻²³ In particular, ternary NiCo₂S₄ has gained a lot of attention due to its excellent electrocatalytic properties which arises from the unique d-electronic configuration of Co (III) at the surface of NiCo₂S₄.²⁴ It possesses richer redox ability than the single phase of metal sulphides due to its synergistic effect from both nickel and cobalt ions and also shows much higher conductivity.^{25, 26} NiCo₂S₄ was first reported as a CE for DSSC by Lin et al., fabricated by using solvothermal and electrophoresis method.²⁷ The resultant NiCo₂S₄ showed the high transmittance (75%) and reached 6.14% efficiency, which is comparable to the conventional Pt CE. Also, nanoneedles of nickel cobalt sulphide are directly fabricated on FTO substrates by a hydrothermal method in the presence of hydrogen sulfide and argon gas mixture and used as CE for DSSCs with the efficiency of 6.9 %.²⁸ Recently, Li et. al reported the low temperature solution process of NiCo₂S₄ nanosheet films converted from NiCo₂O₄ nanosheet films on FTO and employed as CE for p-type DSSCs.²⁹ The dendrite

CSIR-Central Electrochemical Research Institute, Karaikudi 630 006, India, Tel.:+91 4565 241234, 261, Email: mohan40159@cecri.res.in (S. Mohan), skpanda@cecri.res.in (S. K. Panda)

nanostructures have attracted extensive research interests as it possess a large specific surface area of fractals, short diffusion length, and mechanical integrity of the dendrite can provide robust stability by the micro- and nanosized assemblies.³⁰ The structure provides path for the small molecules to penetrate through the branches to reach the internal catalyst surface sites and it can effectively transport holes or electrons via the interconnected networks in the scaffolds.³¹ There are few reports which suggest that electrodeposition is one of the suitable techniques to synthesize dendrite structures directly on a conducting substrate.³²⁻³⁴ To the best of our knowledge, the studies on electrodeposited NiCo₂S₄ towards I₃⁻ reduction in DSSCs have not yet been presented so far. In this study, NiCo₂S₄ is firstly synthesized via a facile one-step electrodeposition route directly onto a FTO glass substrate. The electrochemical deposition is preferred due to its facile and controllable manner for getting the crystallinity, controlled thickness and different morphology through various competing factors and also it does not require high temperature and vacuum conditions. Also this electrodeposition technique provided the direct deposition on FTO substrate which made the fabrication procedure easier for large scale application of DSSCs. We synthesized the NiCo₂S₄ by using both PS and PR technique and investigated their electrochemical performances. When employed as CEs for DSSCs, it exhibited higher cell efficiency than the conventional Pt CEs and the previously reported literatures based on NiCo₂S₄ CEs.^{27, 28}

2. Experimental

2.1. Fabrication of NiCo₂S₄ CEs

All the chemicals were received from Sigma Aldrich and used as received without any further purification. NiCo₂S₄ dendrite nanostructures were deposited on FTO by both potentiostatic (PS) and pulse reverse (PR) electrodeposition method. The electrolyte bath is formulated by taking 5 mM of CoCl₂.6H₂O, 2.5 mM of NiCl₂.6H₂O and 0.75 mM of thiourea and the pH of the solution is measured to be 6.5. The deposition was carried out in a three electrode cell at room temperature using IVIUMSTAT XRI electrochemical workstation. The cleaned FTO serves as a working electrode, Pt counter electrode and Saturated Calomel Electrode (SCE) as a reference electrode. After deposition, the FTO plates were cleaned with deionized water and dried under an air flow.

2.2. Assembly of DSSCs devices

FTO substrates were cleaned in acetone and ethanol mixture (1:1) by ultrasonication. The cleaned FTO substrates were spin coated by 20 mM TiCl₄ aqueous solution and heated at 450 °C for half an hour to make TiO₂ compact layer. After that P25 TiO₂ nanoparticles were coated by doctor blade method by mixing the nanoparticles with polyethylene glycol (mol. wt. 6000), triton X, acetylacetone and deionized water. The coated substrates were heated at 450 °C for one hour in air. After drying, the substrates were soaked in 0.3 mM N719 [di-tetrabutylammonium cis-bis (isothiocyanato) bis (2, 2'-

bipyridyl- 4, 4'-dicarboxylato) ruthenium (II)] dye solution in ethanol for about 24 hours for dye adsorption. The sensitized FTO substrates were washed with ethanol for removing excess dye molecules. The cell dimensions were measured 0.4 x 0.4 cm². The dye sensitized photoanodes were sandwiched with the as deposited NiCo₂S₄ counter electrodes and the red-ox electrolyte (0.1 M I⁻, 0.05 M I₂, 0.6 M 3-methyl n-propyl-imidazolium iodide and 0.5 M tert-butylpyridine in acetonitrile solvent) was injected into the cell through the holes which were already made on FTO substrates by drilling. For comparison, Pt CE was prepared by spin coating method with a solution of chloroplatinic acid (H₂PtCl₆.6H₂O, 50 mM) in isopropyl alcohol on drilled FTO substrate in 1000 rpm and heated at 400 °C for 30 minutes.

2.3. Characterization

The deposited NiCo₂S₄ CEs thin films were characterized for phase formation and phase purity by powder X-ray diffraction (XRD) technique using Cu-K α radiation (D8 Advance, BRUKER). The morphologies of synthesized powder samples were analyzed using TESCAN Scanning Electron Microscope (SEM). The microstructure of PR sample was characterized by TECNAI F20 FTWIN TMP High Resolution Transmission Electron microscope (HR-TEM). For TEM sample preparation, the electrodeposited sample was scratched from FTO substrate and ultrasonicated for few mins in isopropyl alcohol and then drop casted on a copper grid. CV measurements for counter electrode were performed using IVIUMSTAT XRI electrochemical workstation. The photovoltaic properties of the assembled DSSCs were measured by recording the current-voltage characteristics using a potentiostat (VMP3, BIO-LOGIC) under illumination with a Solar Simulator (PHOTOEMISSION TECH) with an AM 1.5G filter set. The intensity of the illumination is 100 mW/cm². The electrochemical impedance spectroscopic (EIS) measurements were made at open circuit voltage conditions under illumination (100 mW/cm²) in the frequency range 0.1 Hz to 1 MHz with an amplitude voltage of 10 mV.

3. Results and Discussion

3.1. Electrochemical growth of NiCo₂S₄ on FTO

To find out the best deposition potential for NiCo₂S₄, Linear Sweep Voltammetry (LSV) was carried out using the aqueous electrolyte containing 5mM CoCl₂.6H₂O, 2.5 mM NiCl₂.6H₂O and 0.75 M thiourea and is shown in Fig. 1a. In the cathodic sweep, the deposition of NiCo₂S₄ starts at -1.16 V, indicating a quite large overpotential which can be assigned to the polarization of Ni²⁺ and Co²⁺ at the FTO surface. Due to hydrogen evolution, the small current is developed before NiCo₂S₄ deposition. However, a small hump is observed at around -0.73 V which indicates the electroreduction of thiourea and incorporation of S into the Ni-Co films. On the other hand, to determine the oxidation potential of deposited Ni and Co in NiCo₂S₄ thin films LSV with anodic sweep has been done (Fig. 1b) using the following three aqueous electrolytes (i) 5 mM CoCl₂.6H₂O, (ii) 2.5 mM NiCl₂.6H₂O (iii) 5 mM

CoCl₂·6H₂O, 2.5 mM NiCl₂·6H₂O and 0.75 M thiourea. The deposition of Co and Ni started at around -0.7 and -0.9 V and the oxidation potential occurred at -0.1 and -0.2 V respectively. The oxidation of both Co and Ni takes place at -0.16 V, which shows the dissolving rate of Co and Ni is greater in the presence of a large amount of thiourea. By applying an anodic bias following the cathodic bias can help to remove the unwanted Co and Ni which is deposited during the cathodic process and the process is known as potential reverse (PR) technique. The repetition of such procedure is useful for

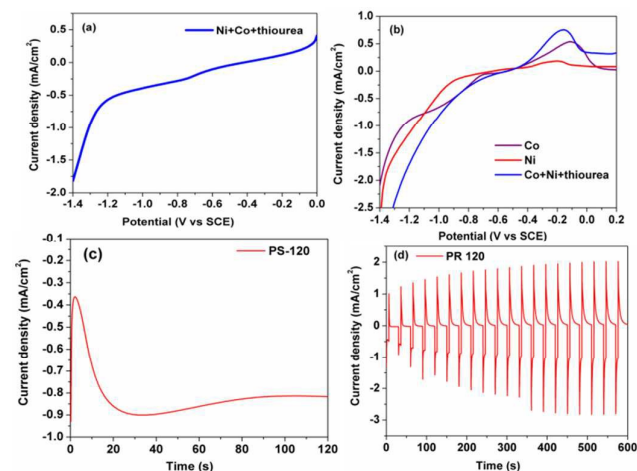


Fig. 1 Linear sweep voltammetry using 5mM CoCl₂·6H₂O, 2.5 mM NiCl₂·6H₂O and 0.75 M thiourea aqueous electrolyte at (a) cathodic sweep mode, (b) anodic sweep mode, (c) I-t curve obtained during deposition using PS technique for 120 s and (d) I-t curve during deposition by PR technique for 20 cycles.

removing the metallic Co and Ni. NiCo₂S₄ CEs are prepared by both PS and PR technique using the electrolyte (iii). The cathodic deposition was carried out at around -1.2 V for both techniques. The NiCo₂S₄ CEs are fabricated by PS technique with the time duration of 60 and 120 s. For PR technique, the anodic and cathodic time was set as 24 s and 6 s respectively and 20 cycles were performed for a total deposition time of 120 s. The PS (60 s, 120 s) and PR (120 s) fabricated NiCo₂S₄ CEs were designated as PS-60, PS-120 and PR-120 respectively.

The current-time (I-t) curves for PS and PR technique are shown in (Fig. 1c and Fig. 1d). In the PS deposition for 120 s (Fig. 1c) the current drops first and then it increases continually. The initial drops is due to the depletion of Ni²⁺ and Co²⁺ ions at the surface of FTO substrate and the increase in current describes the polarization of Ni²⁺ and Co²⁺ ions. In PR technique, the current approaches zero at the end of every anodic polarization which indicates the complete removal of Ni and Co metals. The large cathodic current describes the presence of excess Ni²⁺ ions near the FTO surface caused by the anodic process.

The formation of NiCo₂S₄ on FTO substrate was confirmed by X-ray diffraction studies. Fig. 2 shows the XRD pattern of electrodeposited NiCo₂S₄ thin films by PS-120 and PR-120. All

the reflections were indexed based on the standard pattern of cubic NiCo₂S₄ (JCPDS no. 00-020-0782). The pattern of both films show the planes of (400), (551) and (800), corresponding to a cubic NiCo₂S₄. The cubic phase of metallic Ni and Co was observed on both PS and PR deposited film, but the intensity of the (111) plane is low for PR-120 because of the dissolution of metallic Ni and Co. From these XRD results, the formation of

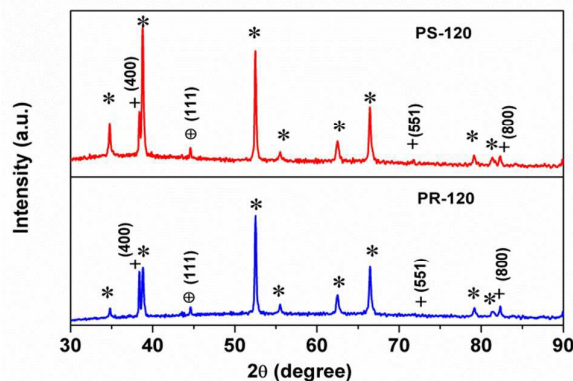


Fig. 2 XRD of electrodeposited NiCo₂S₄ films of PS-120 and PR-120; *: FTO; ⊕: Ni & Co; +: NiCo₂S₄.

NiCo₂S₄ on FTO was confirmed and the removal of metal Ni and Co during the anodic polarization in the PR method was established.

3.2. Morphology studies

Fig. 3 shows the SEM images of electrodeposited NiCo₂S₄ thin films of PS-120 and PR-120 (Fig. 3a and 3c) and the corresponding magnified images are shown in Figure 3b and 3d respectively. In both the PS and PR deposition techniques, dendrite nanostructures were clearly observed on the FTO coated films. PR deposition results in the more oriented flower like fractal morphology. F. Kzuihiro et.al. studied the detailed mechanism for the growth of such dendrite morphology of metals fabricated by electrodeposition method.³⁵ Accordingly, at near equilibrium conditions the surface energy will take a minimum value, while increasing the driving force the flat surfaces become unstable due to the higher contribution of mass or heat diffusion due to this the unstable surface guides the formation of dendrites. In electrochemical deposition, the growth under far equilibrium conditions can be studied by simply altering the electrode potential, current density or concentration of electro-active species. In PR technique, due to the removal of undesired pure Co and Ni metals, the concentration of reacting species is higher near the electrode surface on anodic bias as a result higher current density is necessary for deplete the region near the electrode during cathodic bias.³⁶ Due to the higher mass transport in PR technique, the surface instability increases, which leads to the formation well oriented hyper branched flower like

morphology. The inset of (Fig. 3c) shows the EDX spectrum and it was confirmed the composition of electrodeposited thin films consisting of Ni, Co and S. The high intensity peaks of Si, F, O and Sn elements were from the FTO substrate due to the formation of thin layer of NiCo_2S_4 films. The atomic percentage of Ni, Co and S contents was listed in Table 1. In PS technique, the percentage of Ni and Co gets increased for 60 and 120 s. In

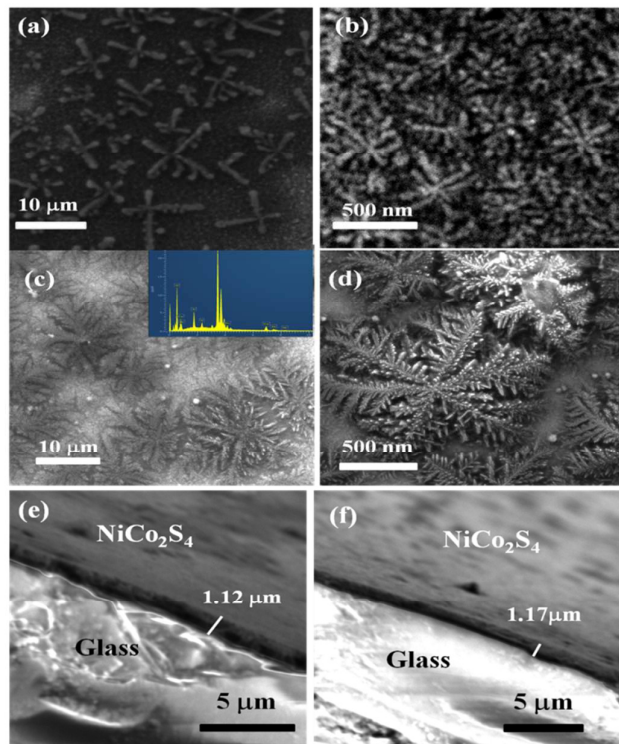


Fig. 3 SEM images of NiCo_2S_4 thin films (a) & (b) PS-120, (c) & (d) PR-120, (e) & (f) cross sectional image of PS-120 and PR-120 respectively. The inset of (c) is the EDAX spectrum of PR-120.

Table 1. Atomic percentage of Ni, Co and S in the NiCo_2S_4 electrodes.

Counter Electrode	Ni	Co	S
PS-60	13.07	26.19	60.74
PS-120	16.67	32.83	50.50
PR-120	15.40	30.41	54.19

the case of PR technique, the atomic percentage of these metals was decreased due to the dissolution of Ni and Co metals during the anodic bias. The thickness of the thin films (PS-120 and PR-120) has been measured by the cross sectional SEM images Fig. 3e and 3f) and the obtained values are 1.12 μm and 1.17 μm for PS-120 and PR-120 respectively indicating deposition of almost same thickness of materials in both the electrodeposition protocols.

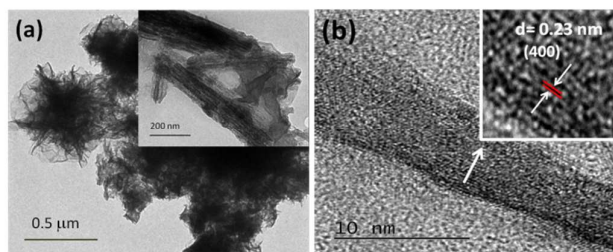


Fig. 4a and 4b HR-TEM images of PR-120 and the inset of Fig. 4a shows the high magnification image.

The low magnification bright field TEM image of the sample PR-120 is shown in Fig. 4a. From the image the branched like morphology is clearly observed and the inset shows the magnified image of one of the branches. The HR-TEM image (Fig. 4b) shows the lattice fringes, which confirms the crystalline nature of the dendrite structures. The inset of Fig. 4b shows the magnified HR-TEM image of one part of the dendrite structure where the lattice fringes were clearly observed. The calculated d-spacing value is ~ 0.23 nm, which is well matching to the (400) plane of NiCo_2S_4 .

3.3. Electrochemical activity and stability of CEs

The catalytic activities towards the reduction of I_3^- in the (I^-/I_3^-) redox couple of the as deposited NiCo_2S_4 and Pt CEs were characterized by cyclic voltammetry (CV) in the acetonitrile solution containing 10 mM LiI , 1mM I_2 , and 0.1 M LiClO_4 at a scanning rate of 50 mV/s and is shown in Figure 5a. The cyclic voltammograms show two typical pairs of oxidation/reduction peaks which were denoted as Ox-A/Red-A and Ox-B/Red-B. Ox-A/Red-A represents the oxidation and reduction of (I^-/I_3^-) couple and Ox-B/Red-B represents the oxidation and reduction of (I_3^-/I_2) couple. The peak current densities of PS-60, PS-120 and PR-120 CEs were raised than that of Pt. It reveals that the oxidation and reduction of (I^-/I_3^-) redox couple has been greatly enhanced at the surface of NiCo_2S_4 CEs, suggesting it as a suitable alternate CE material in DSSCs in place of Pt. To examine the relationship between the scanning rates and peak current densities, CV was performed at different scanning rates for the CEs (Fig. 5b). The transportation of iodide species toward all the CEs is diffusion limited and this was found from the obtained linear relationship between peak current densities and the scan rates. This is due to the fact that, by increasing the scan rate, thin diffusion layer and large electrochemical polarization was obtained, which leads to high overpotential and poor reversibility.³⁷ To find out the stability of the as deposited NiCo_2S_4 CEs (PS-120 and PR-120) toward the (I^-/I_3^-) redox couple, CV was recorded for 20 consecutive cycles at a scan rate of 50 mV/s (Figure 5c and 5d). The constant peak current density and unaltered curve shape demonstrate the awesome electrochemical stability of NiCo_2S_4 CEs in an (I^-/I_3^-) redox couple.

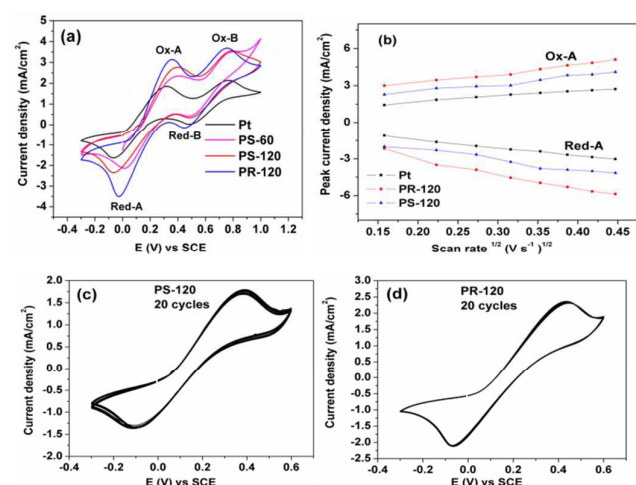


Fig. 5 (a) Cyclic voltammograms of Pt and electrodeposited NiCo_2S_4 CEs at a scan rate of 50 mV/s. (b) Relationship between the peak current density and square root of scanning rate of Pt and NiCo_2S_4 CEs. (c) and (d) 20 consecutive cyclic voltammograms of PS-120 and PR-120 CEs at a scan rate of 50 mV/s respectively.

3.4. Solar cell characterization

The improved catalytic activity and electrochemical stability of deposited NiCo_2S_4 thin films towards (I^-/I_3^-) redox shuttle make it potentially suitable CE material in DSSCs. The photocurrent density-voltage characteristics for the fabricated DSSCs using PS-60, 120, PR-120 and Pt as CEs were evaluated and are shown in Fig. 6a. The corresponding photovoltaic parameters are summarized in Table 2. For all the devices, there is no such variation in the open circuit voltage (V_{oc}) values was observed, because the V_{oc} is mostly depend on the photoanode material and the redox shuttle. But the short circuit current density (J_{sc}) values were increased than the Pt CE, which is due to the fractal like morphology of NiCo_2S_4 that promotes the charge transfer reaction and the higher electrocatalytic activity, which is also supported by the CV measurements (Fig. 6a). Fill factor (FF) is observed to be high for the PR-120 sample than the other CEs. This improvement in FF from 63.8 % to 67.8 % is due to the removal of excess metallic Ni and Co during the PR deposition process. The photovoltaic efficiency of PS-120 and PR-120 was enhanced by 1.05 % and 1.22 % respectively in comparison to the DSSC with Pt CE. Figure 6b shows the long term stability of the fabricated DSSCs for a period of 15 days, which indicates that the efficiency of the cells are almost stable for a long period of time and is also supported by Fig. 5c and 5d.

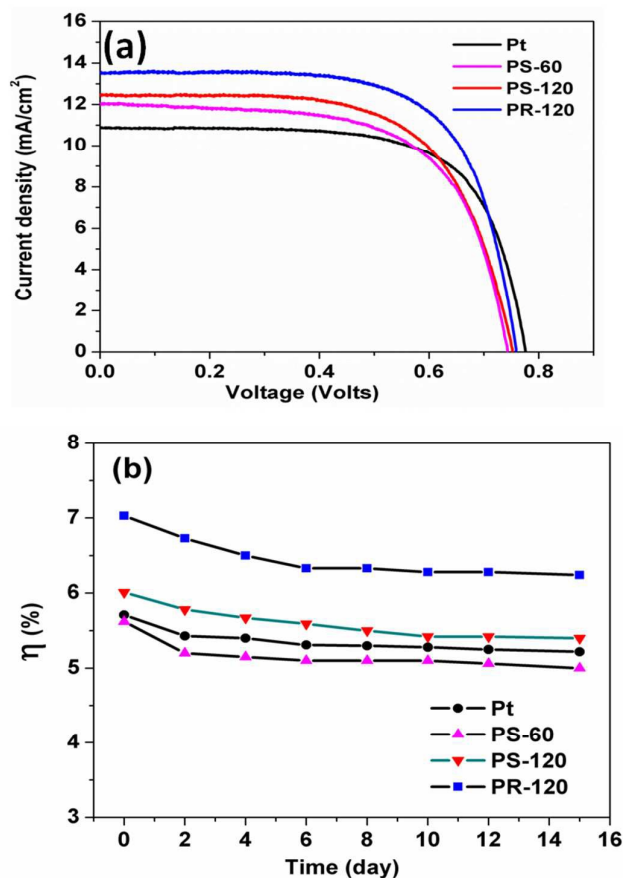


Fig. 6 (a) J-V characteristics of DSSCs using Pt and electrodeposited NiCo_2S_4 counter electrodes and (b) Long term stability of DSSCs employing CEs with Pt, PS-60, PS-120 and PR-120.

Table 2. Photovoltaic parameters obtained from the J-V curves shown in Fig. 5a

Counter Electrode	V_{oc} (mV)	J_{sc} (mA/cm ²)	FF (%)	η (%)
Pt	0.776	10.9	67.6	5.71
PS-60	0.742	11.8	63.9	5.62
PS-120	0.751	12.5	64.0	6.01
PR-120	0.758	13.6	68.1	7.03

3.5. Electrochemical Impedance Studies

The interfacial charge transfer and the kinetics of charge transport at the electrode/ electrolyte interface was studied by Electrochemical Impedance Spectroscopy (EIS) for the fabricated DSSC devices and the obtained Nyquist plot was shown in Fig. 7. The intercept at higher frequency range on the

real axis represents the series resistance (R_s). The left semicircle in higher frequency region demonstrates the charge transfer resistance (R_{ct}) at electrolyte/CE interface and the relative constant phase angle element (CPE). The Nernst diffusion within the electrolyte and charge transfer process at the interface was occurred in the low frequency region and these processes were explained by Warburg impedance, (W), R_{ct} and CPE. The inset of Fig. 7 shows the equivalent circuit used to fit the experimental EIS data and it was fitted by Zsimpwin 3.0 software. The two semicircles were clearly obtained for Pt, PS-60, PS-120, and PR-120 based DSSCs. The obtained parameters (R_s and R_{ct}) from Nyquist plot were listed in Table 3 for Pt, PS-60, PS-120 and PR-120 CEs. Both the R_s and R_{ct} values were decreased for PS-60, PS-120 and PR-120 CEs based DSSCs compared to Pt due to the high surface area of the dendrite structures and the removal of excess Ni and Co during the anodic bias in PR technique. Higher catalytic activities of PS-60, PS-120 and PR-120 CEs have been proved from EIS measurements as also evidenced by CV measurements.

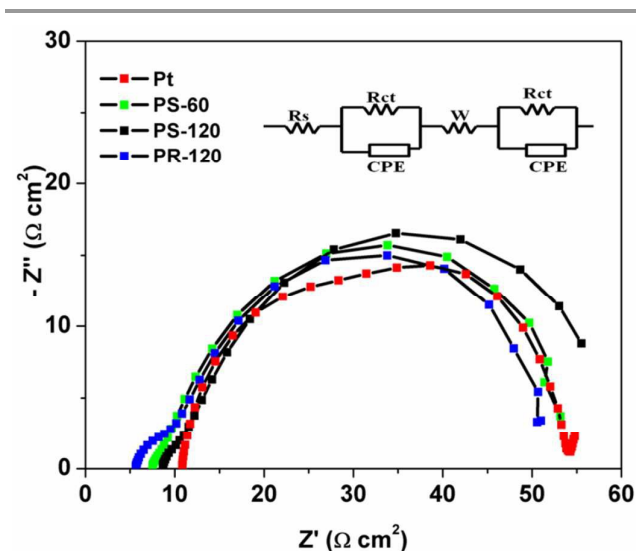


Fig. 7 EIS Nyquist plots of DSSCs using Pt/FTO and electrodeposited NiCo_2S_4 CEs and the inset is the equivalent circuit model.

Table 3. Parameters obtained from EIS measurements for different CEs.

Counter electrode	R_s ($\Omega \text{ cm}^{-2}$)	R_{ct} ($\Omega \text{ cm}^{-2}$)
Pt	9.1	14.1
PS-60	7.42	4.76
PS-120	7.8	4.4
PR-120	5.8	3.9

4. Conclusions

In conclusion, dendrite structured NiCo_2S_4 on FTO substrates were fabricated by facile one-step electrodeposition method using both Potentiostatic and pulse reverse techniques. In the pulse reverse technique due to the periodically imposed anodic bias, excess metallic Ni and Co are removed, which produced more phase pure NiCo_2S_4 . Due to the hyper-branched dendrite morphology, the electrochemical studies revealed the excellent electrochemical activity for (I^-/I_3^-) redox shuttle. The pulse reverse deposited counter electrode shows lower R_{ct} at the counter electrode/electrolyte interface and performed higher efficiency than the conventional Pt counter electrode. Optimization of the electrodeposition parameters may lead to further higher efficiency solar cells. This suggests that the as deposited NiCo_2S_4 counter electrodes by the low-cost and up-scalable electrochemical deposition route are an effective alternate low cost counter electrode material for dye-sensitized solar cell applications.

Acknowledgements

SKP would like to thank Department of Science and Technology, Government of India, for the financial support (Project no: SB/FT/CS-048/2012). Authors also acknowledge CSIR-XII Five Year plan Intel Coat (CSC0114).

References

- B. O'Regan and M. Grätzel, *Nature*, 1991, **353**, 737.
- A. Listorti, B. O'Regan and J. N. Durrant, *Chem. Mater.*, 2011, **23**, 3381.
- K. S. Anuratha and N. Lakshminarasimhan, *J. Solid State Electrochem.*, 2014, **18**, 3407.
- L. Etgar, J. Park, C. Barolo, V. Lesnyak, S. K. Panda, P. Quagliotto, S. G. Hickey, M. K. Nazeeruddin, A. Eychmuller, G. Viscardi, and M. Grätzel, *RSC Adv.*, 2012, **2**, 2748.
- A. Mishra, M. K. R. Fischer and P. Bauerle, *Angew. Chem., Int. Ed.*, 2009, **48**, 2474.
- T. Ma, X. Fang, M. Akiyama, K. Inoue, H. Noma, and E. Abe *J. Electroanal. Chem.*, 2004, **574**, 77.
- S. Yun, A. Hagfeldt and T. Ma, *Adv. Mater.* 2014, **26**, 6210.
- T. N. Murakami and M. Grätzel, *Inorg.Chim. Acta*, 2008, **361**, 572.
- J. Chen, K. Li, Y. Luo, X. Guo, D. Li, M. Deng, S. Huang, and Q. Meng, *Carbon*, 2009, **47**, 2704.
- K-C. Huang, Y-C. Wang, R-X. Dong, W-C. Tsai, K-W. Tsai, C-C Wang, Y-H. Chen, R. Vittal, J-J. Lin and K-C. Ho, *J. Mater. chem.*, 2010, **20**, 4067.
- J. M. Pringle, V. Armel and D. R. MacFarlane, *Chem. Commun.* 2010, **46**, 5367.
- H. C. Sun, D. Qin, S. Q. Huang, X. Z. Guo, D. M. Li, Y. H. Luo and Q. B. Meng, *Energy Environ. Sci.* 2011, **4**, 2630.
- J. S. Jang, D. J. Ham, E. Ramasamy, J. Lee, and L. S. Lee, *Chem. Commun.*, 2010, **46**, 8600.
- G. R. Li, J. Song, G. L. Pan and X. P. Gao, *Energy Environ. Sci.*, 2011, **4**, 1680.
- W. Zhao, T. Q. Lin, S. R. Sun, H. Bi, P. Chen, D. Y. Wan and F.Q. Huang, *J. Mater. Chem. A*, 2013, **1**, 194.
- J. Y. Lin, J. H. Liao and S. W. Chou, *Electrochim. Acta*, 2011, **56**, 8818.

- 17 W. Liu, S. He, T. Yang, Y. Feng, G. Qian, J. Xu and S. Miao *Appl. Surf. Sci.* 2014, **313**, 498.
- 18 S. Li, Z. Chen and W. Zhang, *Mater. Lett.*, 2012, **72**, 22.
- 19 Z. Zhang, X. Zhang, H. Xu, Z. Liu, S. Pang, X. Zhou, S. Dong, X. Chen, and G. Cui *ACS Appl. Mater. Interfaces*, 2012, **4**, 6242.
- 20 J. Xu, X. Yang, Q-D. Yang, T-L. Wong and C-S. Lee, *J. Phys. Chem. C*, 2012, **116**, 19718.
- 21 S. Peng, L. Li, C. Li, H. Tan, R. Cai, H. Yu, S. Mhaisalkar, M. Srinivasan, S. Ramakrishna and Q. Yan, *Chem. Commun.*, 2013, **49**, 10178.
- 22 Q. Liu, J. T. Jin and J. Y. Zhang, *ACS Appl. Mater. Interfaces*, 2013, **5**, 5002.
- 23 J. Wu, S. Dou, A. Shen, X. Wang, Z. Ma, C. Ouyang and S. Wang, *J. Mater. Chem. A*, 2014, **2**, 20990.
- 24 Z. Zhang, X. Wang, G. Cui, A. Zhang, X. Zhou, H. Xu and L. Gu, *Nanoscale*, 2014, **6**, 3540.
- 25 J. F. Li, S. L. Xiong, Y. R. Liu, Z. C. Ju and Y. T. Qian, *ACS Appl. Mater. Interfaces*, 2013, **5**, 981.
- 26 H. C. Chen, J. J. Jiang, L. Zhang, H. Z. Wan, T. Qi and D. D. Xia, *Nanoscale*, 2013, **5**, 8879.
- 27 J-Y. Lin and S-W. Chou, *Electrochem. Commun.*, 2013, **37**, 11.
- 28 A. Banerjee, K. K. Upadhyay, S. Bhatnagar, M. Tathavadekar, U. Bansode, S. Agarkar and S. B. Ogale, *RSC Adv.*, 2014, **4**, 8289.
- 29 Z. Shi, H. Lu, Q. Liu, F. Cao, J. Guo, K. Deng and L. Li, *Nanoscale Res Lett*, 2014, **9**, 608.
- 30 I. Gur, N. A. Fromer, C. P. Chen, A. G. Kanaras and A. P. Alivisatos, *Nano Lett.*, 2007, **7**, 409.
- 31 H. Jung, S. H. Lee, J. Yang, M. Cho and Y. Lee, *RSC Adv.*, 2014, **4**, 47714.
- 32 K-H. Ye, Z-Q. Liu, N. Li, K. Xiao, J. Wang and Y-Z. Su, *J. Electrochem. Soc.* 2012, **159**, D737.
- 33 T. H. Lin, C. W. Lin, H. H. Liu, J. T. Sheu and W. H. Hung *Chem. Commun.*, 2011, **47**, 2044.
- 34 R. Qiu, H.G. Cha, H. B. Noh, Y. B. Shim, X. L. Zhang, R. Qiao, D. Zhang, Y. I. Kim, U. Pal and Y. S. Kang, *J. Phys. Chem. C*, 2009, **113**, 15891.
- 35 K. Fukami, S. Nakanishi, H. Yamasaki, T. Tada, K. Sonoda, N. Kamikawa, N. Tsuji, H. Sakaguchi and Y. Nakato, *J. Phys. Chem. C*, 2007, **111**, 1150.
- 36 J-C. Puippe, F. Leamen, F. *Theory and practice of pulse plating*. American Electroplaters and surface Finishers Society: 1909; chapter 5, pp 65-66.
- 37 X. Zheng, J. Deng, N. Wang, D. Deng, W-H. Zhang, X. Bao and C. Li, *Angew. Chem. Int. Ed.* 2014, **53**, 7023.

Graphical Abstract

Dendrite nanostructures of NiCo_2S_4 fabricated by simple and cost effective electrodeposition method and its performance as a counter electrode in dye-sensitized solar cells.

